UDC 681.518.5:629.735.03 (045)

Sergiy Enchev[1]
Sergiy Tovkach[2]

WAVELET-BASED ALGORITHM FOR DETECTION OF BEARING FAULTS IN A GAS TURBINE ENGINE

National Aviation University
Kosmonavta Komarova avenue 1, 03680, Kyiv, Ukraine
E-mails: [1]esw@ukr.net; [2]tcctit7@ukr.net

Abstract. *Presented is a gas turbine engine bearing diagnostic system that integrates information from various advanced vibration analysis techniques to achieve robust bearing health state awareness. This paper presents a computational algorithm for identifying power frequency variations and integer harmonics by using wavelet-based transform. The continuous wavelet transform with the complex Morlet wavelet is adopted to detect the harmonics presented in a power signal. The algorithm based on the discrete stationary wavelet transform is adopted to denoise the wavelet ridges.*

Keywords: bearing faults; complex Morlet wavelet; gas turbine engine; wavelet scalogram and ridges.

1. Introduction

Improving the reliability and maintainability of gas turbine engines is becoming more critical to end users concerned with reducing costs and increasing availability.

In order to reduce the cost and inconvenience of unscheduled repairs, design engineers have traditionally estimated the statistical reliability of such faulty bearings and assigned a conservative safe life replacement interval (based on time or usage).

However, evidence has indicated that actual usage of military aircraft systems varies considerably depending on intended use and operating environment.

Unanticipated and extreme operating scenarios are major causes of failures and unscheduled maintenance events.

Actual operational lives for aircraft are commonly extended past their original design lives because of the critical mission they perform.

Thus, the unfortunate reality of statistical- based preventative removals is that significant useful life remains in most units while limited failures continue to occur in the field.

The former represents an opportunity to reduce maintenance time and life-cycle costs and increase readiness, while the latter represents a significant opportunity to improve safety through the implementation of diagnostic and prognostic techniques that will enable the transition from the traditional safe life removal/change intervals to condition-based approaches.

A Condition-based Maintenance strategy promises to reduce the costs associated with scheduled maintenance by monitoring the actual condition, or health, of the component and replacing component only when necessary and at optimally scheduled maintenance times.

Vibration-based features are of particular importance in determining the condition of the bearing within this system and are the focus of this paper.

Analysis has shown that vibration features offer better incipient fault detection than the widely used and accepted oil consumed analysis. In addition, vibration-based diagnostics offers isolation capabilities beyond oil debris monitoring [1, 2].

The accuracy of bearing health predictions is critical to a robust and effective Prognostic and Health Management implementation.

Substantial research has focused on the development of robust and accurate features that can be used to increase the accuracy of health predictions; however, many of these developments have occurred in laboratory settings.

Although suitable for proof-of-concept validation, the idealized laboratory test rig is often a simplified form of the target system, such as a gas turbine engine.

Confounding issues, such as indirect vibration transmission path, operating condition issues, and noise sources, are often absent from the development laboratory. Complete validation of the feature or sensor is therefore possible only through actual engine tests.

Therefore, we used data collected from an actual gas turbine engine, mounted in a full scale test cell, to validate the developed techniques.

Some of the results of these tests are presented herein.

2. Analysis of last researches

Solving the problem of synthesis, application efficiency, operation control systems aircraft turbine engine devoted to the work of scientists: V.Y. Berezhnoy [1], O.D. Degtyarev [1], M.M. Kudin [1], O.P. Saveliev [1], A. N. Sinyakov [6], F.A. Shamayrdanov [6], M.S. Kulik [7], J.M. Tereshchenko [7], V.V. Panin [7], S.V. Zhernakov [8].

Bearing failures are of particular concern in high performance turbines because of the potential for catastrophic, cascading consequences throughout the system.

An ability to predict early stage bearing failures will therefore affect turbine reliability and life-cycle costs both positively and dramatically.

Thats why we used wavelet-analysis.

3. Wavelet Transform and analyzing wavelet

Wavelet Transform (WT) has been drawing a lot of attention from scientists and engineers over the years due to its ability to extract time signal and frequency information simultaneously. WT can be continuous or discrete.

Continuous Wavelet Transform (CWT) is adopted for harmonic analysis because of its ability to preserve phase information [2].

The wavelet transform of a continuous signal, $f(t)$, is defined as (1),

$$W\ f(u,s) = \left\langle f, \psi_{u,s} \right\rangle = \int_{-\infty}^{+\infty} f(t) \frac{1}{\sqrt{s}} \Psi^* \left(\frac{t-u}{s} \right) dt,$$

where $\Psi^*(t)$ – the complex conjugate of the wavelet function $\psi(t)$;

s – the dilation parameter (scale) of the wavelet;

u – the translation parameter (location) of the wavelet.

The wavelet function must satisfy certain mathematical criteria [2, 3].

These are the following:

– a wavelet function must have finite energy;

– and u a wavelet function must have a zero mean, that is, has no zero frequency component.

The simplified Complex Morlet Wavelet (CMW) [3, 4] is adopted in the algorithm for harmonic analysis as shown in Fig. 1 and is defined as

$$\Psi(t) = \frac{1}{\sqrt{\pi f_b}} e^{-t^2 / f_b} e^{j 2\pi f_c t}, \quad (1)$$

where f_b – the bandwidth parameter;

f_c – the center frequency of the wavelet.

The CMW is essentially a modulated Gaussian function.

It is particularly useful for harmonic analysis due to its smoothness and harmonic-like waveform.

Because of the analytic nature, CMW is able to separate amplitude and phase information.

Strictly speaking, the mean of the simplified CMW in (1) is not equal to zero as illustrated in

$$\int_{-\infty}^{+\infty} \Psi(t) = \frac{1}{\sqrt{\pi f_b}} \int_{-\infty}^{+\infty} e^{j 2\pi f_c t} e^{-t^2 / f_b} dt = e^{(-f_b/4)(2\pi f_c)^2}. \quad (2)$$

However the mean of the CMW can be made arbitrarily small by picking the f_b and f_c parameters large enough [4, 5].

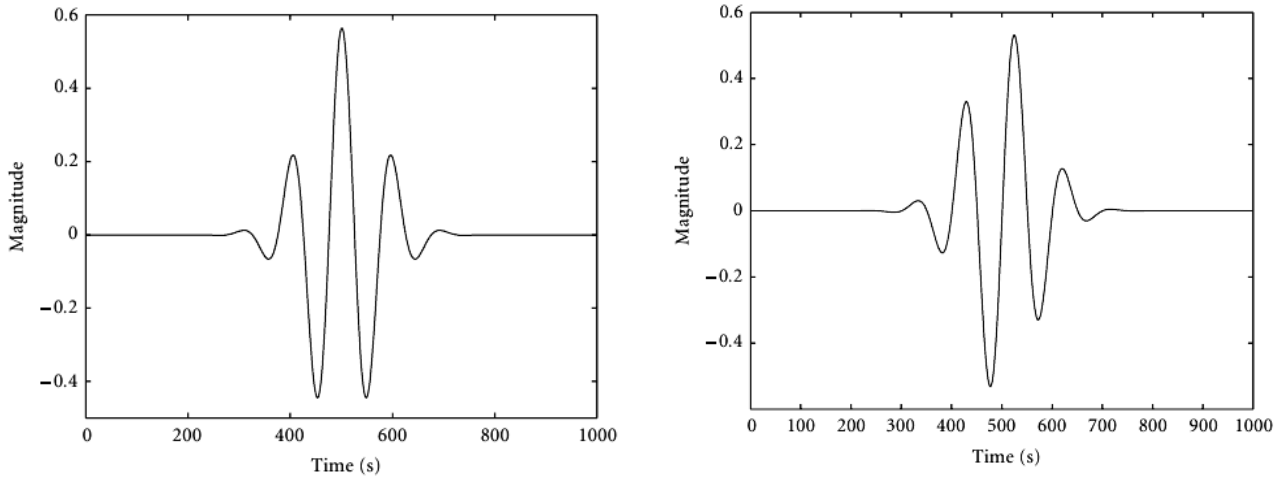

a *b*

Fig. 1. The real part (*a*) and imaginary part (*b*) of the CMW

For example, the mean of the CMW in (2) with $f_b = 2$ and $f_c = 1$ is 2.6753×10^{-9} which is practically equal to zero.

The frequency support of the CMW in (2) is not a compact support but the entire frequency axis.

The effective time support of the CMW in (2) is from -1 to 8 provided that f_b is not more than 9.

From the classical uncertainty principle, it is well known that there is a fundamental trade-off between the time and frequency localization of a signal.

In other words, localization in one domain necessarily comes at the cost of localization in the other.

The time-frequency localization is measured in the mean squares sense and is represented as the Heisenberg box.

The area of the Heisenberg box is limited by

$$\delta\omega\delta t \geq \frac{1}{2},$$

where $\delta\omega$ – the frequency resolution;

δt – the time resolution.

For a dilated complex Morlet wavelet,

$$\delta\omega = \frac{1}{s\sqrt{f_b}},\ \delta t = \frac{s\sqrt{f_b}}{2}. \quad (3)$$

Complex Morlet Wavelet achieves a desirable compromise between time resolution and frequency resolution, with the area of the Heisenberg box equal to 0.5.

From (3), it is seen that the frequency resolution is dependent on the selection of f_b and the dilation.

The dilation is dependent on the selection of f_c and the sampling frequency.

4. Harmonics frequency detection

Given a signal $f(t)$ represented as

$$f(t) = a(t)\cos\phi(t), \quad (4)$$

the wavelet function in (1) can be represented as[5],

$$\psi(t) = g(t)e^{j\omega t}. \quad (5)$$

The dilated and translated wavelet families [4] are represented as

$$\psi_{u,s}(t) = \frac{1}{\sqrt{s}}\psi\left(\frac{t-u}{s}\right) = e^{-j\xi u} g_{s,u,\xi}(t), \quad (6)$$

where

$$g_{s,u,\xi}(t) = \sqrt{s}\, g\left((t-u)/s\right) e^{j\xi t};$$

$$\xi = \omega / s.$$

The wavelet transform of the signal function $f(t)$ in (4) is given as,

$$W f(u,s) = \frac{\sqrt{s}}{2} a(u) e^{j\phi(u)} (\hat{g}(s[\xi - \phi'(u)]) + \varepsilon(u,\xi)), \quad (7)$$

where $\hat{g}(\omega)$ represents the Fourier transform of the function $g(t)$.

The corrective term $\varepsilon(u,\xi)$ in (7) is negligible if $a(t)$ and $\phi'(t)$ in (4) have small variations over the support of $\Psi_{u,s}$ in (6) and if $\phi'(u) \geq \Delta\omega / s$.

If a power signal contains only a single frequency, the corrective term can be safely neglected.

However for a power signal containing harmonics from low frequency to high frequency, the corrective term will contribute to the wavelet coefficients, making the frequency detection not straightforward.

The instantaneous frequency is measured from wavelet ridges determined over the wavelet transform.

The normalized scalogram defined by [2, 5]

$$\frac{\xi}{\eta} P_w f(u,\xi) = \frac{|W f(u,s)|^2}{s} \quad (8)$$

is calculated with

$$\frac{\xi}{\eta} P_w f(u,\xi) = \frac{1}{4} a^2(u) \left| \hat{g}\left(\eta \left[1 - \frac{\phi'(u)}{\xi} \right] \right) + \varepsilon(u,\xi) \right|^2. \quad (9)$$

Since $|\hat{g}(\omega)|$ in (9) is maximum at $\omega = 0$, if one neglects $\varepsilon(u,\xi)$. (9) shows that the scalogram is maximum at

$$\frac{\eta}{s(u)} = \xi(u) = \phi'(u). \quad (10)$$

The corresponding points $(u, \xi(u))$ calculated by (10) are called wavelet ridges [5].

For the CMW, $g(t)$ in (5) is a Gaussian function. Since the Fourier transform of a Gaussian function is also a Gaussian function, the wavelet ridge plot exhibits a Gaussian shape.

Fig. 2 shows the wavelet ridges plot for the 40 Hz signal. It can be seen that the wavelet ridges can accurately detect the signal frequency.

Fig. 3 shows the wavelet ridges plot for the detection of the 40 Hz signal component in the signal containing frequencies at 40 Hz and 240 Hz, respectively.

There are some fluctuations at the peak of the wavelet ridges, introducing small errors in the frequency detection. The fluctuations are due to imperfection of the filters produced by the dilated CMWs and the corrective term in (7).

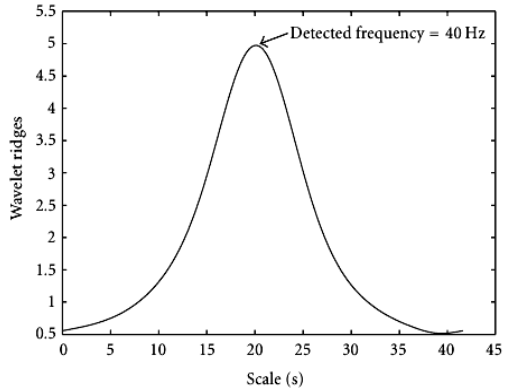

Fig. 2. Wavelet ridges plot for a 40 Hz and 240 signal

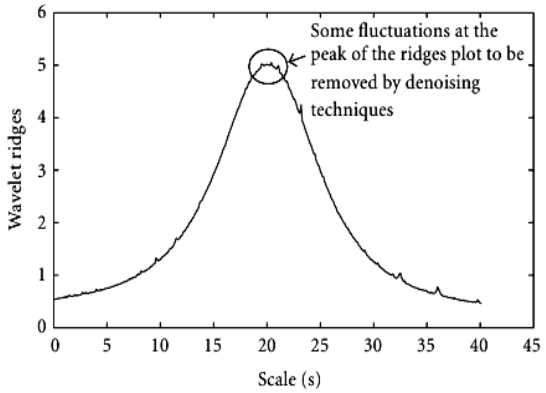

Fig. 3. Wavelet ridges plot for a 40 Hz signal

Discrete Stationary Wavelet Transform (DSWT) [5] is adopted to remove the fluctuations of the wavelet ridges.

In view of the shape of the wavelet ridges, the Symlet2 wavelet developed by Daubechies is used.

It is found that a decomposition level of 5 is sufficient to remove the fluctuations.

Fig. 4 shows the denoised wavelet ridges plot of the signal containing frequencies at 40 Hz and 240 Hz, respectively.

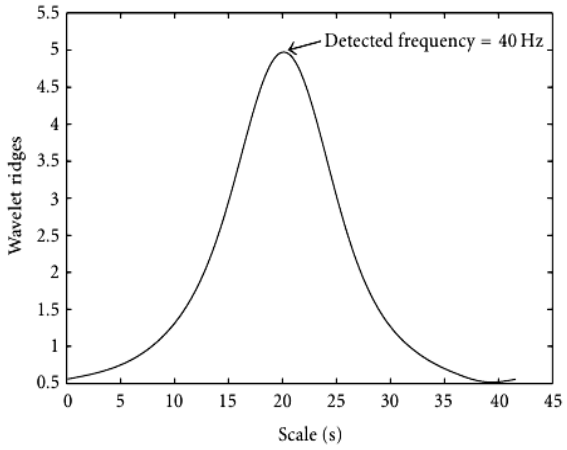

Fig. 4. Denoised wavelet ridges plot of the wavelet ridges plot in Fig. 3

The 40 Hz frequency component of the signal is accurately detected by the wavelet ridges after denoising.

5. Discrimination of adjacent frequencies

The Fourier transform of a dilated CMW in (6) is represented as [1, 6, 7]

$$\Psi(sf) = \sqrt{s}e^{-\pi^2 f_b (sf - f_c)^2}. \quad (11)$$

The function $\psi(sf)$ can be regarded as a bandpass filter centered at the frequency f_c.

The bandwidth of the bandpass filter can be adjusted by adjusting f_b.

The CWT of a signal is the convolution of the signal with a group of bandpass filters which is produced by the dilation of the CMW.

Suppose that (11) is represented as

$$\Psi(sf) = x, \quad (12)$$

where x represents an arbitrary magnitude to be defined later.

Combining (11) and (12) gives

$$f = \frac{f_c}{s} \pm \frac{1}{s\pi\sqrt{f_b}} \sqrt{\left| \ln\left(\frac{x}{\sqrt{s}} \right) \right|}, \quad (13)$$

where f_c / s – the center frequency of the dilated bandpass filter; and the bandwidth is

$$(2/s\pi\sqrt{f_b})\sqrt{\left|\ln(x/\sqrt{s})\right|}.$$

Fig. 5. Shows the plot of the frequency support of two dilated CMWs at scales S_1 and S_2, respectively.

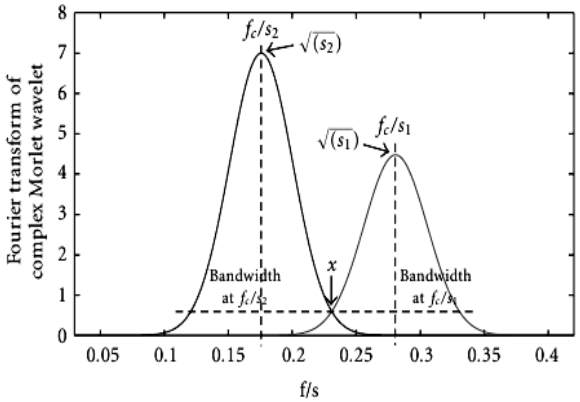

Fig. 5. Frequency plot of (15) for two CMWs at scales S_1 and S_2, respectively

If the two dilated CMWs are used to detect two adjacent frequencies in a signal, with their frequencies represented as

$$f_1 = \frac{f_s f_c}{S_1}, \quad f_2 = \frac{f_s f_c}{S_2},$$

where f_s represents the sampling frequency, then

$$\frac{f_c}{S_1} - \frac{f_c}{S_2} = \frac{1}{S_1 \pi \sqrt{f_b}} \sqrt{\left| \ln\left(\frac{x}{\sqrt{S_1}} \right) \right|} + \frac{1}{S_2 \pi \sqrt{f_b}} \sqrt{\left| \ln\left(\frac{x}{\sqrt{S_2}} \right) \right|}. \quad (14)$$

Assume that $S_2 > S_1$ (14) is simplified to

$$f_c \sqrt{f_b} > \frac{1}{\pi} \sqrt{\left| \ln\left(\frac{x}{\sqrt{S_1}} \right) \right|} x \frac{f_2 + f_1}{f_2 - f_1}. \quad (15)$$

For $S_1 = 200$ and $x = 0.5$,

$$\frac{1}{\pi} \sqrt{\left| \ln\left(\frac{x}{\sqrt{S_1}} \right) \right|} = 0.58. \quad (16)$$

Substituting (16) into (15) gives

$$f_c \sqrt{f_b} > 0.58 x \frac{f_2 + f_1}{f_2 - f_1}, \quad S_1 \le 200, \quad x \le 0.5. \quad (17)$$

It is estimated that the magnitude of x should not be more than 0.5.

Equation (17) is used to determine the values of f_b and f_c in (1) for the continuous wavelet transform with CMW which is a necessary condition to discriminate adjacent frequencies contained in the power signal.

6. Harmonics amplitude detection

Theoretically, once the algorithms developed in 3 and 4 detect the harmonics contained in the power signal, the corresponding harmonics amplitudes would be determined readily by

$$a(u) = \frac{2\sqrt{(\xi/\eta) P_w f(u,\xi)}}{|\hat{g}(0)|} = \frac{2\sqrt{|W f(u,s)|^2 / s}}{1} = \frac{2|W f(u,s)|}{\sqrt{s}}. \quad (18)$$

The values of $2\sqrt{|W f(u,s)|^2 / s}\,2$ in (18) are obtained in the process of generating the scalogram.

Due to the imperfection of the filters produced by the dilated CMWs and the corrective terms in (7), the amplitudes detected exhibit fluctuations.

Simulation results show that the amplitudes for harmonics frequencies from 50 to 1000 Hz have errors of the order of ±5 %.

Fig. 6 shows a plot of the absolute wavelet coefficients generated by (18) for a 991.5 Hz harmonic frequency component of a power signal containing frequencies ranging from 50 to 1000 Hz.

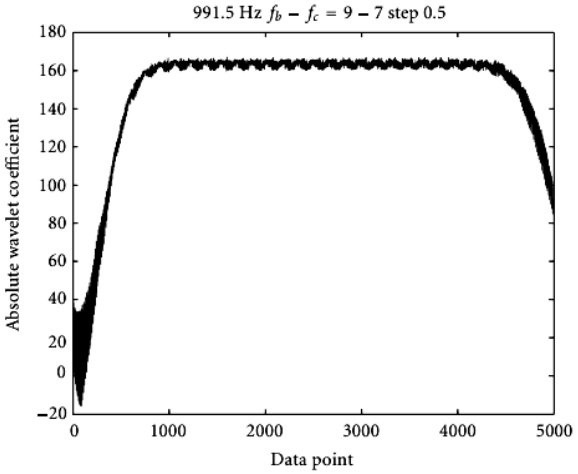

Fig. 6. Absolute wavelet coefficients plot generated by CWT (using complex Morlet wavelet, $f_b = 9$, $f_c = 7$) for harmonic frequency at 991.5 Hz

The smoothness of the absolute wavelet coefficients plot is also related to the number of data points taken per cycle of the harmonic frequency component.

It is found that a minimum of 25 data points per cycle should be used to provide a smoother absolute wavelet coefficients plot.

Discrete Stationary Wavelet Transform [2, 5] is adopted to remove the fluctuations.

Since the absolute wavelet coefficients plot should exhibit a constant magnitude for a harmonic frequency of constant amplitudes, the Haar wavelet is used for the DSWT to denoise the absolute wavelet coefficients. It is found that a decomposition level of 5 is sufficient for harmonics up to 1000 Hz.

Fig. 7 shows the output of the DSWT of the absolute wavelet coefficients shown in Fig. 6.

The fluctuations are removed resulting in an accurate detection of the amplitude of the harmonics frequency.

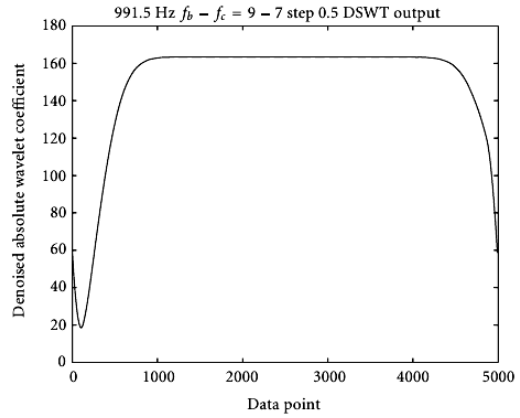

Fig. 7. Coefficients generated by DSWT (Haar wavelet, level 5 decomposition) of the absolute wavelet coefficients plot in Fig. 6

The proposed harmonics detection algorithm is presented in Fig. 8.

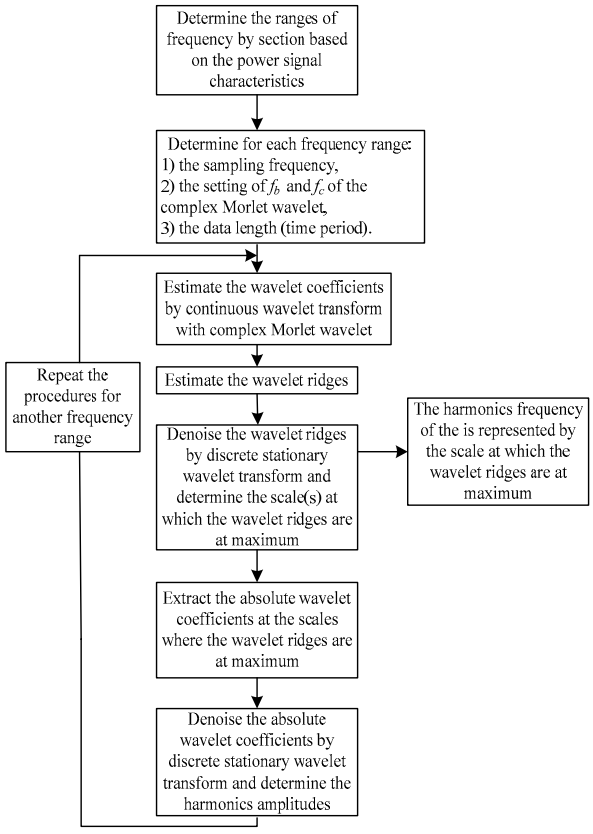

Fig. 8. The flow chart of the proposed harmonics detection algorithm

The proposed algorithm is implemented with Matlab software.

7. Experimental results

In order to characterize various bearing damage levels in the engine, tests were performed with three different bearings.

All bearings tested were gas generator shaft (engine) bearings, from the second bearing location.

First, a healthy bearing with no faults was used to generate baseline data.

Second, a bearing with a seeded inner raceway fault was used to generate incipient fault data.

The fault on the second bearing was seeded by placing two dents (Brinell marks) in the anticipated load path of the bearing (Fig. 9).

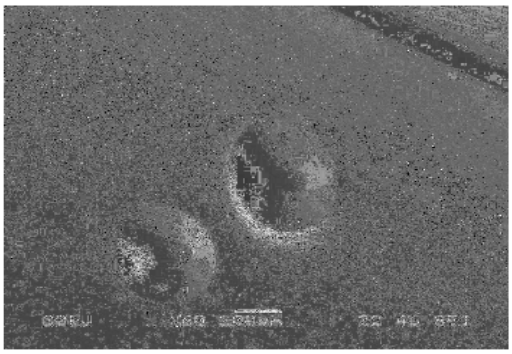

Fig. 9. Dented Inner Raceway

The intent of the marks was to cause the initiation and progression of a spall during testing to characterize fault progression.

The third bearing used in testing had a large, pre-existing spall on the inner raceway and was used to generate data representative of a severe fault.

When applied to bearing vibration signals, autocorrelation is used to estimate the periodicity of the demodulated signals resulting from ImpactEnergy™, WT, or Short Time Energy (STE) processing [6, 8].

The top plot of Fig. 10 is the STE of a wavelet coefficient with center frequency of 18.8 kHz, which was decomposed from the bearing vibration signal as shown in Fig. 11.

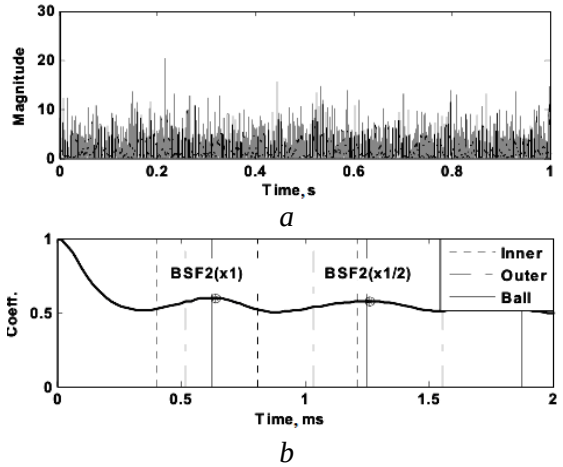

Fig. 10. Demodulation of Bearing Vibration Signal and Fault Detection:
a − STE of a wavelet with center frequency of 18.8 kHz;
b − autocorrelation coeffcient of STE

The bottom plot of Fig. 11 shows the autocorrelation coefficients of the STE and demonstrates that the first and second peaks of the coefficients match the lines of ball defect harmonics, which is indicative of a ball defect.

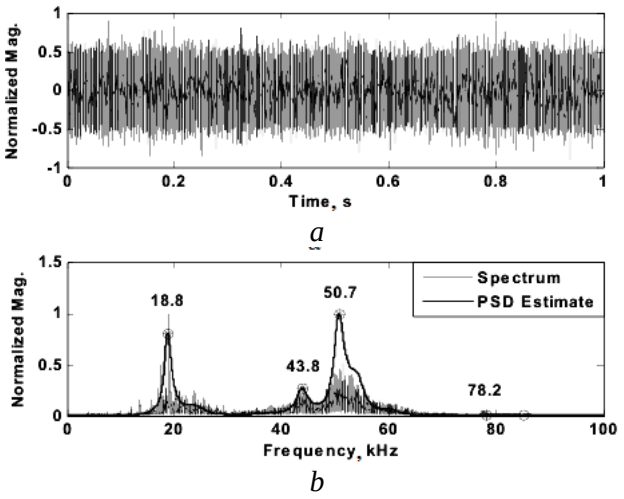

Fig. 11. Band Selection Using a Parametric Method:
a − time waveform of bearing vibration;
b − band selection

For each bearing condition, multiple test cycles were performed.

Two cycles were run on the healthy bearing, which translated to approximately 1 hour of test time.

Sixty-six cycles were run on the dented bearing, which translated to approximately 43 h of test time.

Test time on the spalled bearing was limited due to concerns about the rapid spall progression.

Four cycles, approximately 2 h, were run on the prespalled bearing.

More cycles were put on the dented bearing to initiate, and hopefully propagate, the dent into a spall.

Each of the aforementioned diagnostic techniques was then applied to the collected data.

Successful diagnostic features need the ability to detect an anomaly in the monitored system with minimal false alarms, isolate potentially faulted components, and provide useable correlations to system health [8].

The following sections detail the diagnostic capabilities of the various developed techniques.

Results presented are from a single accelerometer location (gearbox) and only from the high speed and load condition (military power).

This is because the gearbox accelerometer provided the clearest indication of the fault. In addition, the feature magnitudes varied the least during military power, resulting in more robust diagnostic features.

Also, the signal's modulation was more pronounced during military power than during the other regimes.

To establish ground truth, the raceways were visually inspected twice during and once after the testing was complete.

Upon final inspection of the dented raceway, spall initiation and slight progression was witnessed (Fig. 12 as compared to Fig. 9).

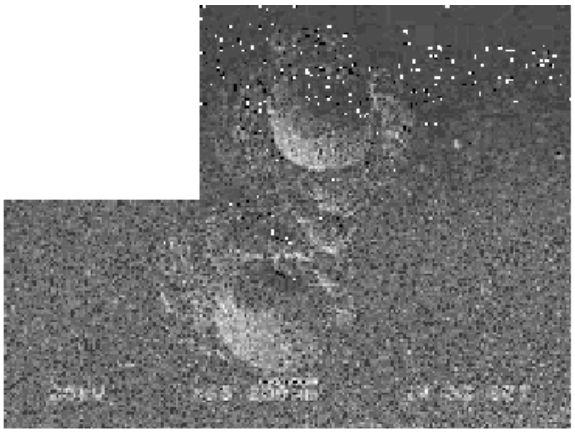

Fig. 12. Dented Raceway End of Testing

Although the spall had progressed, it was still a very small, incipient fault.

Please note that the results shown here are from only during military power, which the engine was run at for 375 min (the total run time was 2400 min).

The feature trend shown in the following figures is divided into stages to investigate the shifts in feature distribution as the test progressed.

The stages correspond to intermediate teardown inspections of the engine to document the fault progression.

8. Conclusions

As part of this work, conventional and new signal processing techniques were combined in different ways to detect bearing faults.

These methods were applied to data collected from baseline and seeded fault bearing tests to verify the efficacy of the integrated techniques.

The proposed harmonics detection algorithm is able to identify the frequency and amplitude of harmonics in a power signal to a very high accuracy.

The accuracy of the proposed harmonic detection algorithm has been verified by tests conducted on a computer-simulated signal and a field signal.

Two techniques are adopted to achieve accurate frequency identification.

Firstly, complex Morlet wavelet is used for the continuous wavelet transform and secondly, wavelet ridges plot is used to extract the frequency information.

Given that the complex Morlet wavelet is a Gaussian modulated function, the area of the Heisenberg box on the time-frequency plane is equal to 0.5.

The bandwidth of the complex Morlet wavelet can be adjusted by carefully selecting the bandwidth determined accurately without the need of a large time window.

It is seen that the wavelet ridges plot is a Gaussian; the scale at which the wavelet ridges plot is maximal represents the frequency of the harmonics in the signal.

Discrete stationary wavelet transform is used to remove small fluctuations near the peak of the wavelet ridges plot so that a smooth Gaussian-like wavelet ridges plot is revealed, the peak of the wavelet ridges plot can then by identified.

Discrete stationary wavelet transform is proved to be useful in denoising the absolute wavelet coefficients of the continuous wavelet transform for amplitudes detection.

The disadvantage of the proposed algorithm is that the accuracy of both frequency and amplitude detections is dependent on the data points taken per cycle of the highest harmonics in the signal.

In other words, a higher sampling frequency than twice the Nyquist frequency is required.

It is concluded that bearing fault detection is highly affected by the hybrid diagnostic techniques that are implemented, as well as the bandwidths chosen for scrutiny.

In other words, the proper selection of the vibration bands and diagnostic techniques will result in better estimation of bearing health.

References

[1] *Berezhnoy, V.Y.; Degtyarev, O.D.; Kudin, M.M.; Saveliev, O.P.* The use of modern methods of analysis for the study of non-stationary signals for vibration GTE on transients.Aerospace engineering and technology. 2008. N 10 (57). P. 184–187 (in Russian).

[2] *Carmona, R. A.; Hwang, W. L.; Torresan, B.* Characterization of signals by the ridges of their wavelet transforms. IEEE Transactions on Signal Processing. 2005. Vol. 45, N 10. P. 2586–2590.

[3] *Defect detection of rolling bearings (translated materials of company IRD)*. Available from Internet: <http://www.vibration.ru/obnar_defekt.shtml> (in Russian).

[4] *Huang, S.-J.; Hsieh, C.-T.; Huang, C.-L.* Application of Morlet wavelets to supervise power system disturbances. IEEE Transactions on Power Delivery. 2009. Vol. 14, N. 1. P. 235–241.

[5] *Pham, V. L.;Wong, K. P.* Wavelet-transform-based algorithm for harmonic analysis of power system waveforms. IEE Proceedings: Generation, Transmission and Distribution. 2007. Vol. 146, N 3. P. 249–254.

[6] *Sinyakov, A. N.; Shamayrdanov, F. A.* Automatic control system of aircraft and propulsion systems. Mechanical engineering. 1991. P. 320 (in Russian).

[7] *Tereshchenko, J. M.; Kulik, M. S.; Panin, V. V.* Theory of aviation gas turbine engine. 2005. P. 500 (in Russian).

[8] *Zhernakov S. V.* Algorithms for control and diagnostics of aircraft gas turbine engine conditions onboard implementation based on neural network technology. 2010. N 3 (38). P. 42-56 (in Russian).

Received 7 April 2014.

С.В. Єнчев[1], С.С. Товкач[2]. Вейвлет-алгоритм для визначення дефектів підшипників у газотурбінному двигуні
Національний авіаційний університет, просп. Космонавта Комарова, 1, Київ, Україна, 03680
E-mails: [1]esw@ukr.net; [2]tcctit7@ukr.net

Розглянуто систему виявлення зароджуваних дефектів підшипників у газотурбінних двигунах за рахунок підвищення надійності та ремонтопридатності літака. Описано діагностичну систему підшипників газотурбінного двигуна, яка об'єднує інформацію з різних сучасних методів аналізу вібрації для досягнення надійного їх стану. Наведено обчислювальний алгоритм для визначення потужності коливання частоти і гармонік із використанням вейвлет-перетворення. Показано, що неперервне вейвлет-перетворення з використанням комплексного вейвлета Морле можливо застосовувати для виявлення гармонік, які подані в потужності сигналу. Алгоритм виявлення частоти розроблено з вейвлет-скалограм і хребтів. Зазначено, що необхідною умовою є розрізнення сусідніх частот. Запропоновано метод миттєвої частотної ідентифікації для визначення компонентів частот. Алгоритм на основі дискретного вейвлет-перетворення використано для зменшення шуму вейвлет-хребтів.
Ключові слова: вейвлет-скалограми і хребти; газотурбінний двигун; дефекти підшипників; комплексний вейвлет Морле.

С.В. Енчев[1], С.С. Товкач[2]. Вейвлет-алгоритм для обнаружения дефектов подшипников в газотурбинном двигателе
Национальный авиационный университет, просп. Космонавта Комарова, 1, Киев, Украина, 03680
E-mails: [1]esw@ukr.net; [2]tcctit7@ukr.net

Рассмотрена система выявления зарождающихся дефектов подшипников в газотурбинных двигателях за счет повышения надежности и ремонтопригодности самолета. Описана диагностическая система подшипников газотурбинного двигателя, объединяющая информацию из различных современных методов анализа вибрации для достижения надежного их состояния. Приведен вычислительный алгоритм для определения мощности колебания частоты и гармоник с использованием вейвлет-преобразования. Показано, что непрерывное вейвлет-преобразование с использованием комплексного вейвлета Морле можно применять для обнаружения гармоник, которые представлены в мощности сигнала. Алгоритм обнаружения частоты разработан на основе вейвлет-скалограмм и хребтов. Отмечено, что необходимым условием является определение соседних частот. Предложен метод мгновенной частотной идентификации для определения компонентов частот. Алгоритм, основанный на дискретном вейвлет-преобразовании, принят для снижения шума вейвлет-хребтов.
Ключевые слова: вейвлет-скалограммы и хребты; газотурбинный двигатель; дефекты подшипников; комплексный вейвлет Морле.

Enchev Sergiy (1979). Candidate of Engineering. Associate Professor.
Automation and Energy Management Department, National Aviation University, Kyiv, Ukraine.
Education: National Aviation University, Kyiv, Ukraine (2002).
Research area: methods of synthesis and diagnostics of power systems control aircraft.
Publications: 111.
E-mail: esw@ukr.net

Tovkach Sergiy (1989). Postgraduate student.
Automation and Energy Management Department, National Aviation University, Kyiv, Ukraine.
Education: Cherkasy National University named after Bohdan Khmelnytsky, Cherkasy, Ukraine (2011).
Research area: the automated processing of measurement data in electronic control systems of aircraft gas turbine engine.
Publications: 18.
E-mail: tcctit7@ukr.net